

ORBITS OF FOUR YOUNG TRIPLE-LINED MULTIPLE SYSTEMS

ANDREI TOKOVININ

Cerro Tololo Inter-American Observatory, Casilla 603, La Serena, Chile
Draft version May 17, 2018

ABSTRACT

Each of the nearby triple systems HIP 7601, 13498, 23824, and 113597 (HD 10800, 18198, 35877, 217389) consists of solar-type dwarfs with comparable masses, where all three components are resolved spectrally, while the outer pairs are resolved both visually and spectrally. These stars are relatively young (between 100 and 600 Myr) and chromospherically active (X-ray sources), although they rotate slowly. Spectroscopic orbits of the inner subsystems (periods 19.4, 14.1, 5.6, 20.3 days) and orbits of the outer systems (periods 1.75, 51, 27, 500 yrs, respectively) are determined. For HIP 7601 and 13498, the combined spectro-interferometric outer orbits produce direct measurement of masses of all components, allowing comparison with stellar models. The 6708Å lithium line is present and its strength is measured in each component individually by subtracting the contributions of other components. The inner and outer orbits of HIP 7601 are nearly circular, likely co-planar, and have a modest period ratio of 1:33. This study contributes to the characterization of hierarchical multiplicity in the solar neighborhood and provides data for testing stellar evolutionary models and chronology.

Subject headings: stars: binaries

1. INTRODUCTION

Binary and multiple stars attract interest for various reasons. Historically, they served as excellent calibrators of stellar masses, radii, and other parameters, e.g. for testing and refining evolutionary models. Multiple systems also host interesting processes such as dynamical interactions, mass transfer, mergers, etc. Multiplicity statistics and studies of certain key objects inform us on the processes of star formation. The objects featured in this work are interesting from several points of view.

Radial velocities (RVs) of nearby solar-type multiple systems were monitored in 2014 and 2015 to determine the frequency of spectroscopic subsystems in visual components and to follow their orbital motion. The resulting statistics were reported in (Tokovinin 2015), while detailed analysis of individual systems was deferred to future publications. This paper is the first of this series. It deals with four triple-lined spectroscopic binaries (SB3s). These solar-type multiple systems (Table 1) are relatively young, as inferred from chromospheric activity (all are X-ray sources) and the presence of lithium. The first two objects were identified as SB3s by Wichman et al. (2003) in a spectroscopic follow-up of *ROSAT*. The wide common-proper-motion (CPM) pair HIP 113579 and 113597 belongs to the AB Doradus association (Torres et al. 2006); its fainter component is the SB3. In all four SB3s, the outer subsystems are spatially resolved; their orbits in the plane of the sky are computed or updated here together with spectroscopic orbits of the inner subsystems.

In this work, I designate individual components of hierarchical multiples by sequences of letters such as A, Ab or AB; a component may contain one or several stars. The binary systems are designated by joining components with comma, e.g. Aa,Ab. The designation A,B stands for the binary system with two components A and B, while the designation AB stands for one component,

e.g. an unresolved binary in a system AB,C.

The observational material and data analysis are presented in Section 2. Sections 3 to 6 are devoted to the individual systems and follow the same template: bibliography, orbits, and estimation of component's parameters. In Section 7, the results are used to discuss the mass-luminosity relation, strength of the lithium line, and origin of hierarchical triple-lined systems. The last Section 8 summarizes the paper.

2. OBSERVATIONS AND DATA ANALYSIS

2.1. Spectroscopic observations

Most spectra used here were taken with the 1.5-m telescope located at the Cerro Tololo Interamerican Observatory in Chile and operated by the SMARTS Consortium.¹ The observing time was allocated through NOAO (programs 14B-0009, 15A-0055, 15B-0012). The observations were made with the fiber-fed echelle spectrograph CHIRON² (Tokovinin et al. 2013) by the telescope operators in service mode. The spectra taken in the slicer mode have a resolution of $R = 80,000$ and a signal to noise ratio of at least 20. They cover the range from 415 nm to 880 nm in 53 orders. Thorium-argon calibrations were recorded for each target. A few spectra taken in 2010 at the same telescope with the Fiber Echelle (FECH) with a resolution of $R = 44,000$ (Tokovinin et al. 2015a) are used here, too. Most (but not all) individual RVs are published in (Tokovinin 2015), where preliminary orbital periods are also announced.

2.2. Radial velocities by cross-correlation

The reduced and wavelength-calibrated spectra delivered by the CHIRON pipeline were retrieved from the SMARTS center at the Yale University. The availability of this service has greatly enhanced this program by al-

¹ <http://www.astro.yale.edu/smarts/>

² <http://www.ctio.noao.edu/noao/content/chiron>

Table 1
Basic parameters of multiple systems

HIP	HD	WDS (J2000)	Spectral type	V (mag)	$B - V$ (mag)	μ_α^* (mas yr $^{-1}$)	μ_δ	π_{HIP2}^a (mas)
7601	10800	01379–8258	G1V	5.87	0.62	+122	+120	36.52 ± 0.28
13498	18198	02539–4436	K0III?	7.73	0.69	+107	+56	14.09 ± 0.73
23824	35877	05073–8352	F8V	6.80	0.57	+57	+147	20.81 ± 0.48
113579	217343	23005–2619	G5V	7.47	0.64	+7	–108	32.51 ± 0.71
113597	217379	23005–2619	K7V	9.65	1.34	+14	–157	32.74 ± 2.03

^a Proper motions and parallax from HIP2 (van Leeuwen 2007).

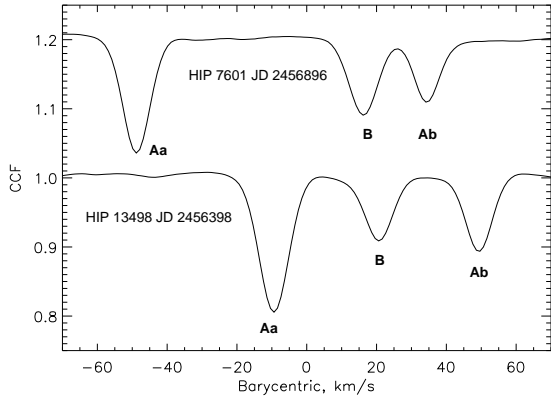


Figure 1. CCFs of triple-lined systems HIP 7601 (upper curve, shifted by 0.2) and HIP 13498 (lower curve). The letters mark components corresponding to each CCF dip.

lowing rapid analysis of the RVs and flexible scheduling of new observations when needed.

The spectra were cross-correlated with the digital binary mask (template) based on the solar spectrum stored in the NOAO archive (see Tokovinin et al. 2015a, for more details). The cross-correlation function (CCF) $C(v)$ is computed over the RV span of $v = \pm 200 \text{ km s}^{-1}$ in the spectral range from 4500\AA to 6500\AA . CCFs of all orders are simply summed up and normalized by the median value. Portions of the CCFs within $\pm 2.35\sigma$ of each dip are approximated by Gaussian curves. After the first iteration, the centers and dispersions are determined, and in the second iteration the fitting area is adjusted accordingly. The CCF model with three Gaussians is

$$C(v) = 1 - \sum_{j=1}^3 a_j \exp[-(v - v_j)^2 / 2\sigma_j^2]; \quad (1)$$

it contains nine free parameters (v_j, a_j, σ_j). CCFs with overlapping (blended) dips were processed by fixing amplitudes a_j or dispersions σ_j to the values determined on other nights from well-resolved CCFs, like those in Figure 1.

I do not provide formal errors of RVs and of other parameters resulting from the CCF fits, as they are very small and do not characterize the real precision of the results. The RV precision is dominated by systematic effects and is estimated from residuals to the orbits at $\sim 0.1 \text{ km s}^{-1}$. The velocity zero point relies on the wavelength calibration and on the mask derived from the solar spectrum, rather than on standard stars.

2.3. Estimation of rotation velocity

The CCF width σ depends on the spectral resolution, correlation mask, and the intrinsic width of stellar lines. The latter are broadened by rotation, macro-turbulence, and other factors. When rotation dominates, the CCF shape deviates substantially from a Gaussian, but for moderate or slow rotation the CCF is well modeled by a Gaussian with increased dispersion σ . I calibrated the relation between the projected rotation speed $V \sin i$ and σ using digital solar spectrum. It was broadened by a Gaussian PSF corresponding to the spectral resolution $R = 80,000$ (3.75 km s^{-1}) and rotation (e.g. Díaz et al. 2011), assuming a linear limb darkening law with a coefficient of 0.65. The broadened spectrum was correlated with the mask. After accounting for the solar rotation of 2 km s^{-1} , the results can be fitted by the formula

$$V \sin i \approx 1.80 \sqrt{\sigma^2 - \sigma_0^2}, \quad (2)$$

where $\sigma_0 = 3.4$ and all values are in km s^{-1} . This relation is valid for $\sigma < 12$ and is accurate to ± 0.4 , as long as line broadening factors other than rotation are same as in the Sun. In the fiber mode of CHIRON, not used here, $\sigma_0 = 5.4$ and the coefficient is 1.92. This approximate method cannot replace detailed analysis of line profiles, but it is suitable for multiple stars with solar-type components studied here. Disentangling of spectra will be needed for a more refined determination of rotation and other stellar properties.

2.4. Speckle interferometry

Information on the resolved outer subsystems is retrieved from the Washington Double Star Catalog, WDS (Mason et al. 2001). It is complemented by recent speckle interferometry at the SOAR telescope. The latest publication (Tokovinin et al. 2015c) contains references to the previous papers of this series. Observations made in 2015 and 2016 are not yet published.

2.5. Orbit calculation

Orbital elements and their errors were determined by the least-squares fits with weights inversely proportional to the adopted data errors. The IDL code `orbit`³ was used. It can fit spectroscopic, visual, or combined visual/spectroscopic orbits. Formal errors of orbital elements are determined from these fits. The errors of masses and orbital parallax derived from combined orbits are computed by taking into account correlations between individual elements.

Orbits of the subsystems were determined iteratively. Knowing the semi-amplitudes K_1 and K_2 in the inner

³ <http://www.ctio.noao.edu/~jatokovin/orbit/>

orbit Aa,Ab, I estimate the RV of A (center of mass) as the weighted sum, $V_A = (K_2 V_{Aa} + K_1 V_{Ab}) / (K_1 + K_2)$. These RVs together with the RVs of the secondary component B and the speckle measurements define the outer orbit. The V_A resulting from the motion in the outer orbit is then subtracted from V_{Aa} and V_{Ab} in the next iteration of the inner orbit, so its center-of-mass velocity γ is zero by definition.

Spectroscopic orbital elements derived in this work are listed in Table 2, the visual orbits are assembled in Table 3, in common notation. For circular orbit, $\omega = 0$ means that the element T corresponds to passage through the node (maximum RV). The last two columns of Table 2 give the weighted rms residuals to the spectroscopic orbits and the total number of RVs for both components. The last column of Table 3 contains the number of astrometric measures. The combined orbits are featured in both tables, duplicating overlapping elements. In combined orbits, the longitude of periastron ω_A corresponds to the primary, and the position angle of the visual orbit Ω_A is chosen accordingly to describe the motion of the secondary. The weights of positional measurements and RVs are balanced, so that each data set has $\chi^2/N \sim 1$, where N is the number of degrees of freedom.

The observations used in orbit calculations are listed in two tables, published in full electronically. Table 4 gives, for each date, the RVs of the primary and secondary components V_1 and V_2 , their errors used for relative weighting, and residuals to the orbit O–C. The first column contains the *Hipparcos* number, the second column identifies the system. For the inner subsystem of HIP 7601, the velocities V_1 and V_2 are relative to the center-of-mass V_A (motion in the visual orbit is subtracted). In the outer orbits, V_1 refers to the center of mass of the subsystem. The last column of Table 4 specifies the data source. RVs of the non-variable component HIP 113597B are also listed in this Table.

The resolved astrometric measurements are listed in Table 5 in a similar way as the RVs, with the first two columns identifying the system. Then follow the date, position angle θ , separation ρ , position error σ_ρ used for weighting, residuals to the orbit, and reference.

2.6. System modeling

Individual magnitudes of the components are computed from the relative areas of their CCFs which are proportional to the product $a\sigma$. Although spectral types of all components in SB3s are similar, a small correction is needed to account for the dependence of the line strength on effective temperature. Using synthetic spectra (Berthone et al. 2008), I found that the CCF surface depends on the effective temperature T_e almost linearly, proportional to $1 - 3.27(T_e/6000 - 1)$ for $4000 < T_e < 6500$. At lower T_e the surface decreases. The measured CCF areas are corrected for this factor, assuming a reasonable T_e , to split the combined V -band flux between the components. Resolved photometry of visual pairs is used as an independent check. The CCF parameters and magnitudes of individual components are given in Table 6.

The *Hipparcos* distance modulus gives absolute magnitudes of the components, so their masses are estimated using standard relations (e.g. Henry & McCarty

1993; Tokovinin 2014a) or Dartmouthh isochrones (Dotter et al. 2008), assuming that the stars are on the main sequence. Effective temperatures and individual magnitudes in different filters are then derived from the masses with the help of the same standard relations, and the combined photometry resulting from the system model is compared to the actual combined magnitudes. This provides a check on the temperatures. The modeled masses are compared to the dynamical mass sum from the visual orbit or to the actually measured masses from the combined orbit. Adjustments to the model are made iteratively to achieve a better match between observed and modeled properties of each system; the details are different, depending on the available data.

The guesswork of matching data and models cannot replace actual measurement of stellar parameters. However, it is useful for detecting discrepancies and for estimating parameters not measured directly, such as effective temperatures and colors of individual components. To distinguish model-dependent (estimated) parameters, they are marked by asterisks in the tables.

2.7. The lithium line

Presence of the resonance lithium doublet at 6707.761Å and 6707.912Å (average wavelength 6707.82Å) in the spectra of solar-type stars is a sign of their relatively young age (Soderblom et al. 1993). Unfortunately, this line is located near the end of the CHIRON echelle order. Its quantitative analysis in SB3s is complicated because the line is a blend of three components in orbital motion. The following procedure was used.

The echelle order containing the lithium line was normalized by the fitted continuum. Nominal positions of the 6707.82Å line corresponding to each component were computed using their measured RVs and the barycentric correction. The expected profiles of the lithium-line blend computed with preliminary estimates of its amplitudes and widths for each component matched the individual spectra quite well. Then I reconstructed the line profile of each component by subtracting the contributions of the other two components from each spectrum, shifting the resulting spectrum to the rest-frame wavelength, and averaging all spectra with weights proportional to the flux. The primary component with the strongest lithium line is processed first, using preliminary estimates for the other two components. Then the line profile of the second component is reconstructed in the same way, using the refined estimate of the primary. Finally, the weakest component is retrieved by subtracting the first two.

The lithium line in the co-added spectrum of each component is fitted by a Gaussian curve to measure its amplitude a_{Li} , width σ_{Li} , equivalent width EW_{Li} , and wavelength λ_{Li} . The latter shows that the lines are indeed not shifted from the assumed rest-frame wavelength of 6707.82Å. The measured EWs are divided by the relative flux of each component f_R to make the result comparable to the line strength in single stars. The R -band magnitudes derived from the system models are used for this correction. Note that the lithium line is wider than the CCF, being a blend of two lines spaced by 6.7 km s⁻¹.

Table 2
Spectroscopic orbits

HIP <i>HD</i>	System	P (d)	T (+24 00000)	e	ω_A (deg)	K_1 (km s ⁻¹)	K_2 (km s ⁻¹)	γ (km s ⁻¹)	rms _{1,2} (km s ⁻¹)	$N_{1,2}$
7601 <i>10800</i>	Aa,Ab	19.37128 ±0.00005	56938.599 ±0.021	0.1028 ±0.0009	242.8 ±0.4	36.45 ±0.04	43.32 ±0.05	0.0 fixed	0.12 0.15	19 17
7601 <i>10800</i>	A,B	638.67 ±0.17	56903.42 ±0.94	0.1912 ±0.0018	151.2 ±0.3	9.10 ±0.03	17.91 ±0.05	-1.65 ±0.02	0.08 0.13	19 20
13498 <i>18198</i>	Aa,Ab	14.0921 ±0.0025	56974.21 ±0.02	0.328 ±0.005	19.3 ±1.1	41.96 ±0.31	48.66 ±0.34	17.78 ±0.08	0.06 0.10	9 9
13498 <i>18198</i>	A,B	18794 ±301	54190 ±49	0.774 ±0.013	16.2 ±1.8	3.98 ±0.61	9.93 ±0.70	18.61 ±0.11	0.03 0.03	10 9
23824 <i>35877</i>	Aa,Ab	5.6310 ±0.0003	57372.683 ±0.003	0 fixed	0 fixed	54.72 ±0.22	61.64 ±0.22	1.29 ±0.12	0.12 0.16	11 9
23824 <i>35877</i>	A,B	9857 ±206	56783.1 ±6.6	0.654 ±0.007	70.7 ±0.9	4.55 ±0.29	11.78 ±0.26	4.60 fixed	0.00 0.20	11 9
113597 <i>217379</i>	Aa,Ab	20.3490 ±0.0002	57255.941 ±0.032	0.433 ±0.003	43.4 ±0.6	41.06 ±0.23	43.62 ±0.23	7.56 ±0.11	0.55 0.49	18 16

Table 3
Visual orbits

HIP <i>HD</i>	System	P (yr)	T (yr)	e	a (arcsec)	Ω_A (deg)	ω_A (deg)	i (deg)	N
7601 <i>10800</i>	A,B	1.74861 ±0.00047	2014.672 ±0.003	0.1912 ±0.0018	0.07823 ±0.00047	296.0 ±0.3	151.2 ±0.3	47.60 ±0.48	14
13498 <i>18198</i>	A,B	51.46 ±0.82	2007.24 ±0.14	0.774 ±0.013	0.2967 ±0.0044	298.3 ±1.3	16.2 ±1.7	49.5 ±1.9	17
23824 <i>35877</i>	A,B	26.99 ±0.56	2014.34 ±0.02	0.654 ±0.006	0.2742 ±0.0040	2.4 ±0.7	70.7 ±0.9	61.6 ±0.50	11
113597	A,B	500	1843.2	0.55	2.46	250.1	150.0	80.9	14

Table 4
Radial velocities and residuals (fragment)

HIP	System	Date (JD +2400000)	V_1	σ_1 (km s ⁻¹)	$(O-C)_1$	V_2	σ_2 (km s ⁻¹)	$(O-C)_2$	Ref. ^a
7601	Aa,Ab	54855.5390	20.426	0.100	0.147	-24.180	0.200	-0.080	H
7601	Aa,Ab	57352.5730	31.592	0.100	-0.004	-37.246	0.150	0.304	C
7601	Aa,Ab	57365.5720	-7.403	0.100	-0.087	8.838	0.150	0.144	C
7601	A,B	51845.2470	-12.060	2.000	-0.009	18.700	1.000	-0.110	W
7601	A,B	54782.5586	6.040	1.000	0.580	-15.950	1.000	-0.308	L
7601	A,B	54855.5386	2.225	0.080	0.171	-9.147	0.200	-0.207	H
7601	A,B	56896.8139	-10.712	0.080	-0.041	16.253	0.150	0.159	C

^a C: CHIRON; E: Elliott et al. (2014); F: FECH; H: HARPS; L: Tokovinin (2015); W: Wichman et al. (2003).

Table 5
Position measurements and residuals (fragment)

HIP	System	Date (yr)	θ (°)	ρ ($''$)	σ ($''$)	$(O-C)_\theta$ ($''$)	$(O-C)_\rho$ ($''$)	Ref. ^a
7601	A,B	2011.0366	50.2	0.0378	0.020	-3.7	-0.0096	SOAR
7601	A,B	2011.0366	53.4	0.0488	0.010	-0.5	0.0014	SOAR
7601	A,B	2014.7661	113.0	0.0640	0.001	-3.0	-0.0004	SOAR
13498	A,B	1927.0200	126.4	0.390	1.050	0.3	-0.125	Vis
13498	A,B	1990.9160	139.2	0.444	0.005	0.1	0.004	Spe
13498	A,B	1991.2500	140.0	0.437	0.010	0.5	0.002	Hip

^a HIP: Hipparcos; SOAR: speckle interferometry at SOAR; Spe: speckle interferometry at other telescopes; Vis: visual micrometer measures.

Table 6
CCF parameters and V magnitudes

HIP	Comp.	a	σ (km s ⁻¹)	$a\sigma$ (km s ⁻¹)	V (mag)
7601	Aa	0.164	3.79	0.620	6.64
7601	B	0.115	4.16	0.477	7.08
7601	Ab	0.086	3.56	0.307	7.74
13498	Aa	0.192	4.15	0.795	8.31
13498	Ab	0.106	3.75	0.397	9.36
13498	B	0.092	3.93	0.360	9.52
23824	Aa	0.133	5.21	0.690	7.30
23824	Ab	0.089	4.61	0.411	8.13
23824	B	0.042	3.52	0.151	9.61
113597	Aa	0.212	5.24	1.111	10.64
113597	Ab	0.130	5.57	0.724	10.80
113597	B	0.081	5.96	0.483	11.09

3. HIP 7601 (HD 10800)

The G1V star HIP 7601 (HR 512) is located at a distance of 27 pc from the Sun; it is designated as GJ 67.1 in the catalog of nearby stars. According to Wichman et al. (2003), it is a young SB3 system and an X-ray source. Nordström et al. (2004) recognized it as a double-lined binary. This bright star has an extensive literature. Its chromospheric activity was measured by Henry et al. (1996), $\log R'(HK) = -4.6$. These authors noted that the star is slightly more active than normal, but not *very* active. There is no obvious emission in the core of the H α line. Torres et al. (2006) detected the lithium line 6707.8Å and measured its equivalent width of 70 mÅ, indicative of a young age. Based on the *IRAS* photometry, a mid-IR excess at 25 μ m was detected, suggesting a debris disk. However, further observations at the VLT have shown no mid-IR excess at 11.59 μ m and 18.72 μ m (Smith et al. 2008). Incidentally, there were no other faint stars within the 19'' field of view. Trilling et al. (2008) also found no energy excess in the *Spitzer* passbands; the flux at 70 μ m was even less than predicted by the photospheric model.

Physical parameters of the star were derived from high-resolution spectra by several authors, apparently disregarding its multiplicity. Maldonado et al. (2012) determined the metallicity $[\text{Fe}/\text{H}] = -0.11$ and age $\log t = 9.09$. Ammler-von Eiff & Reiners (2012) found projected rotational velocity $V \sin i = 1.8 \pm 0.6$ km s⁻¹. Casagrande et al. (2011) give $T_e = 5905$ K, $[\text{Fe}/\text{H}] = -0.13$, $\log g = 4.06$, while Saffe et al. (2008) determined $T_e = 5901$ K, $\log g = 4.84$, $[\text{Fe}/\text{H}] = +0.09$. The triple-lined nature of the spectrum could potentially bias these results.

All three dips in the CCF are narrow, differing in their contrast (Figure 1). The dip amplitudes of Aa, B, and Ab (strongest to weakest) and the widths of their CCFs σ , determined only from the triple-lined (not blended) spectra and averaged, are listed in Table 6. The σ correspond to $V \sin i$ of 3.0, 4.3, and 1.8 km s⁻¹ in Aa, B, and Ab, respectively (see Section 2.3).

The outer system was resolved by speckle interferometry at SOAR in 2014 and got the WDS designation J01379–8259 or TOK 426 (Tokovinin et al. 2015c). Archival speckle observation made in 2011, distorted by telescope vibrations, was re-processed and used here in the orbit calculation, as well as the recent yet unpublished speckle measures. The median magnitude differ-

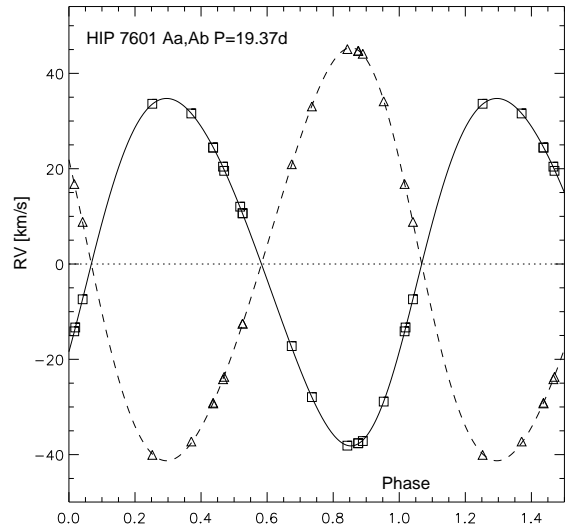


Figure 2. Orbit of the inner subsystem HIP 7601 Aa, Ab. Squares and triangles denote RVs of the primary Aa and the secondary Ab, respectively. Motion in the outer orbit has been subtracted.

ence is 0.79 mag at both 540 and 770 nm wavelengths. The relative photometry is based on 4 and 5 measurements in each band, with the rms scatters of 0.12 and 0.09 mag. The V -magnitudes in Table 6 correspond to $\Delta V_{AB} = 0.77$ mag, in agreement with the speckle photometry.

I found in the ESO archive 11 spectra of HIP 7601 taken with HARPS in the period from 2009 to 2012 (program 088C.513 and its continuation). The spectral resolution is very similar to CHIRON, $R = 80,000$. The reduced spectra were retrieved from the archive and cross-correlated with the solar mask to derive the RVs. Use of these additional data does not increase the time base, but reduces the errors of the orbital elements. I applied a correction of -0.25 km s⁻¹ to these RVs, determined from the γ -velocity of Aa, Ab fitted to the HARPS data alone. RVs derived from blended CCFs are not used in the determination of the inner orbit and are given a low weight (large errors in Table 4) in the outer orbit. The adopted errors of the RVs match the actual rms residuals, yielding $\chi^2/N \sim 1$.

The orbit of the inner subsystem Aa, Ab is shown in Figure 2, and the combined spectro-interferometric orbit of the outer pair A, B is featured in Figure 3. In the final iteration of the outer orbit, I added with a low weight the RVs from Wichman et al. (2003) measured in 2000, $-5.4, -20.6, +18.4$ km s⁻¹ for Aa, Ab, and B, respectively. The spectrum taken in 2008 (Tokovinin et al. 2015a) was also used, although it shows only double lines (two components were blended). The rms residuals to the SOAR speckle measures are 1° in angle and 1.2 mas in separation. The 1.75-yr outer period is determined with a relative error of 0.027 per cent, or just 4 hours.

The combined orbit of A, B leads to the orbital parallax of 37.10 ± 0.45 mas, in good agreement with the HIP2 parallax of 36.52 ± 0.28 mas. The HIP2 parallax corresponds to the mass sum of $3.25 M_{\odot}$, while the orbital masses of A and B are 2.033 ± 0.049 and $1.033 \pm 0.026 M_{\odot}$. Using the mass ratio $q = 0.841$ in the inner orbit, the masses of Aa and Ab are determined as 1.104 ± 0.027 and $0.929 \pm 0.022 M_{\odot}$. Uncertainty of the orbital in-

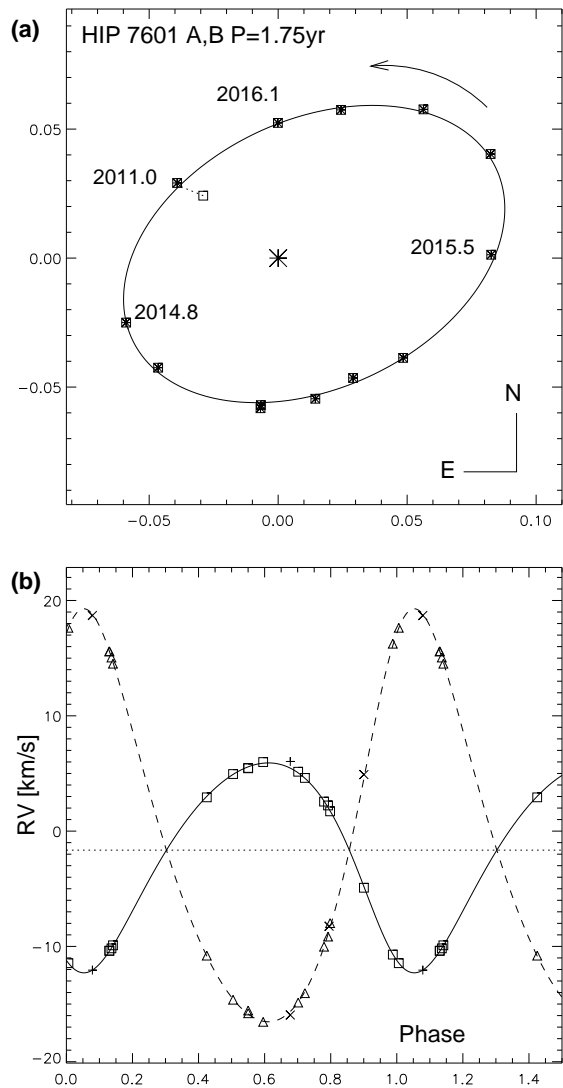


Figure 3. Combined orbit of the outer system HIP 7601 A,B. Top (a): orbit in the plane of the sky, with primary component A at the coordinate origin and scale in arcseconds. Bottom (b): the RV curve (squares for the center-of-mass A, triangles for B). RVs with low weight are plotted as crosses.

clination $i_{A,B}$ contributes to the errors of orbital masses and parallax.

By comparing the sum of orbital masses of Aa and Ab with $M \sin^3 i = 1.00 \mathcal{M}_\odot$ in the inner orbit, its inclination $i_{Aa,Ab} = 51^\circ 9'$ is derived. It is similar to the inclination of $47^\circ 4'$ in the outer orbit; the two orbits thus could be close to co-planarity. The ratio of periods is 32.970 ± 0.009 . Its difference from the integer number 33 is small, although formally significant. An almost integer period ratio and orbits with low eccentricities that are likely co-planar make this system similar to HD 91962, the “planetary” quadruple with a period ratio of 19.0 (Tokovinin et al. 2015b).

The masses and V -magnitudes of all three stars are measured, the distance is known, so the absolute magnitudes M_V are known, too. They match well empirical relations between mass and absolute magnitude M_V , while the Dartmouth isochrones predict M_V that are 0.2 mag too bright (see Section 7.1). To evaluate effective tem-

Table 7
Components of HIP 7601

Parameter	Aa	B	Ab
Mass (\mathcal{M}_\odot)	1.10	1.03	0.93
M_V (mag)	4.45 ± 0.03	4.89 ± 0.03	5.55 ± 0.02
T_e^* (K)	6131	5879	5524
$(B - V)^*$ (mag)	0.50	0.64	0.79
λ_{Li} (Å)	6707.82	6707.82	6707.83
a_{Li}	0.137 ± 0.003	0.058 ± 0.002	0.019 ± 0.002
σ_{Li} (km s $^{-1}$)	5.25	5.71	4.23
	± 0.13	± 0.25	± 0.58
EW_{Li} (mÅ)	40.3	18.6	4.5
f_R^*	0.46	0.33	0.21
$EW_{Li,corr}$ (mÅ)	91.3	56.7	20.6

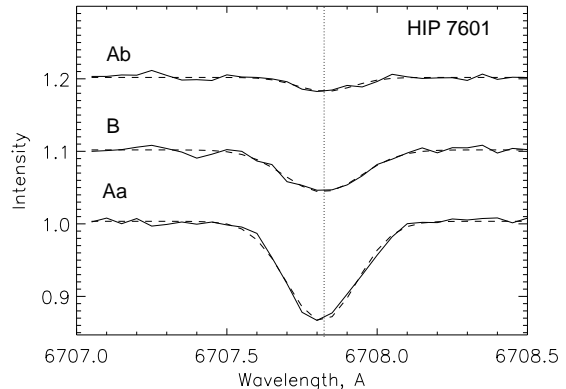


Figure 4. Average spectrum in the region of the lithium line for each component of HIP 7601, with the other two components subtracted. The curves (top to bottom, shifted vertically for clarity) correspond to Ab, B, and Aa. Full lines show the spectra, dashed lines are Gaussian fits. Statistical errors are ± 0.005 .

peratures and colors, I interpolated the solar-metallicity isochrone using masses reduced by 5%. The resulting parameters are listed in Table 7, marked by asterisks to show that they are guessed rather than measured. They lead to the combined $B - V$ and $V - K_s$ colors of 0.60 and 1.44 mag, respectively, while the actual colors are 0.62 and 1.47 mag. The flux-weighted $T_e = 5939$ K is close to $T_e \approx 5900$ K reported in the literature. This agreement indicates that the guessed temperatures of the stars are close to reality.

The profiles of the lithium line in the individual components (Figure 4) are symmetric (no apparent blends) and not shifted in wavelength with respect to their expected position. The nine individual spectra summed in the combined profile have a total flux of 45 000 electrons per pixel, hence the signal-to-noise ratio (SNR) of 210. The sum of the EWs is 63.4 mÅ, in good agreement with 70 mÅ measured by Torres et al. (2006). In the last line of Table 7 the measured EWs are divided by the relative flux of each component f_R , making the result directly comparable to single stars. The component Ab is measured with the largest error owing to the small amplitude of its lithium line and the large correction.

The spatial velocity of HIP 7601 calculated using the γ -velocity of A,B is $(U, W, V) = (-20.0, -2.4, -9.6)$ km s $^{-1}$ (the U axis points away from the Galactic center). It corresponds to the kinematics of young disk. The velocity

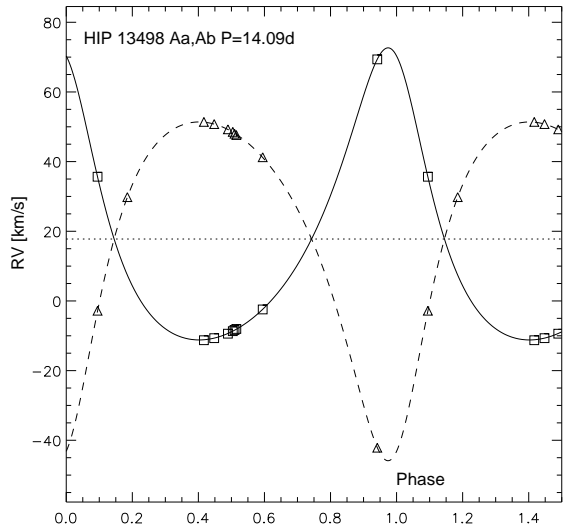


Figure 5. Spectroscopic orbit of HIP 13498 Aa,Ab, $P = 14.09$ d.

is accurate to better than 1 km s^{-1} . The object does not belong to any known kinematic group. The closest kinematic neighbor is probably the Castor group with $(U, W, V) = (-10.7, -7.5, -8.8) \text{ km s}^{-1}$. According to Klutsch et al. (2014), the probability of the HIP 7601’s membership in the Castor group could be around 20%, considering the velocity dispersion of its known members.

4. HIP 13498 (HD 18198)

The star has a spectral type G8/K1III+F: in SIMBAD (Houk 1978), while in fact it consists of three main-sequence dwarfs. Its color is $B - V = 0.69$ mag. The HIP2 parallax is $14.09 \pm 0.73 \text{ mas}$, the original HIP1 parallax is $14.87 \pm 1.13 \text{ mas}$. It is a visual binary I 1480 (WDS J02539–4436) with an orbital period of 52 yr, semi-major axis of $0''.27$, and high eccentricity $e = 0.83$ (Hartkopf et al. 2012). There are no other visual components in the WDS. Wichman et al. (2003) discovered double lines and concluded that there is a spectroscopic subsystem. They measured the lithium line with an equivalent width of $110 \text{ m}\text{\AA}$ (sum of both components) and computed the relative X-ray flux $\log L_X/L_{\text{bol}} = -4.76$. Double lines were also noted by Nordström et al. (2004). Tokovinin et al. (2015a) detected triple lines, implying that all three components have comparable luminosities. The physical parameters were derived from high-resolution spectra, apparently disregarding the multiplicity, by Casagrande et al. (2011) who give $T_e = 5925 \text{ K}$, $[\text{Fe}/\text{H}] = 0.14$, $\log g = 4.03$.

Relative photometry of the outer system A,B by speckle interferometry at SOAR gives the median magnitude differences of 1.52 and 1.49 mag at 540 and 770 nm, respectively. Wichman et al. (2003) list the resolved *Tycho* photometry of A and B reduced to the standard B, V system: $V = (7.97, 9.54)$ mag and $B - V = (0.67, 0.79)$ mag, while $\Delta H_{\text{PAB}} = 1.58$ mag. The resolved photometry indicates that the component B is slightly redder than A. The V -magnitudes in Table 6 correspond to $\Delta V_{\text{AB}} = 1.53$ mag.

After the initial orbital solutions were derived from the CHIRON data, I included the RVs measured in 2008 (Tokovinin et al. 2015a), with a correction to account for

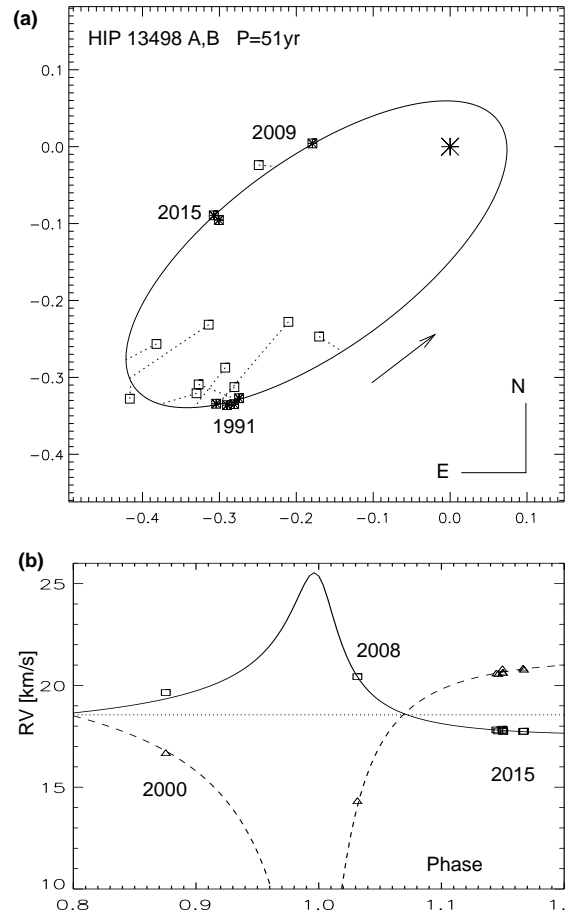


Figure 6. Combined orbit of HIP 13498 A,B (I 1480), $P = 51$ yr. Positions on the sky (a, top) have scale in arcseconds; the empty squares denote visual measurements, the filled squares are accurate data from speckle and *Hipparcos*. Fragment of the RV curve is shown at the bottom (b).

the visual orbit and a correction of $+0.5 \text{ km s}^{-1}$ for the instrument zero point. The 14-day orbit of Aa,Ab is determined quite reliably, with the rms RV residuals of 60 and 100 m s^{-1} for Aa and Ab, respectively.

Using the available micrometer and speckle measurements, the RVs of A (center-of-mass of Aa,Ab) and B, I computed the combined visual/spectroscopic orbit of A,B (Figure 6). The node of the visual orbit is now defined. The weighted rms residuals in angle and separation are $0''.6$ and 3 mas, respectively, while the weighted RV residuals for A and B are 35 and 33 m s^{-1} . The spectrum obtained by Wichman et al. (2003) on 2000.829 (JD 2451847.307) has a strong line with $RV = 12.9 \text{ km s}^{-1}$ (apparently a blend of Aa and B) and a weaker line at 31.2 km s^{-1} that corresponds to Ab. Owing to unresolved blending, this observation is of little help for orbit refinement; it is used with a low weight for the orbit of A,B.

The periastron of the A,B orbit in 2007.3 has not been covered either by speckle observations (back then, time allocation committees denied access of speckle instruments to 4-m telescopes) or by radial velocities (I have not found any spectra in the ESO archive). The next periastron passage will happen in 2058, when the RV difference between A and B will reach 23 km s^{-1} . Available data loosely define the RV amplitudes because the

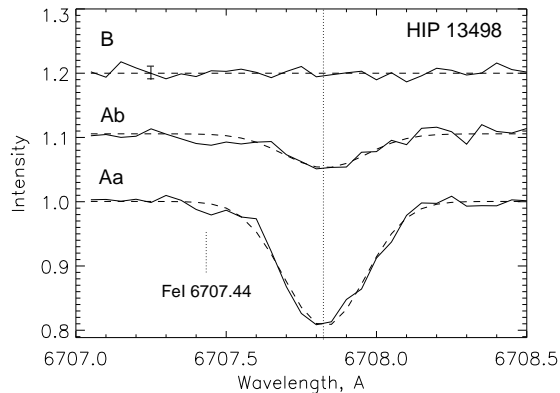


Figure 7. Average spectrum in the region of the lithium line for components of HIP 13498. The full lines show the data, the dashed lines are Gaussian fits.

shape of the RV curve is poorly constrained. Decreasing the element ω_A by only 2° increases the mass sum by $0.6 M_\odot$. The unconstrained orbit in Tables 2 and 3 yields the orbital parallax $\pi_{\text{orb}} = 14.8 \pm 0.8 \text{ mas}$ and the masses $M_A = 2.16 \pm 0.40 M_\odot$ and $M_B = 0.87 \pm 0.25 M_\odot$. This is close to the HIP1 parallax, which I adopt here. The HIP2 parallax leads to the dynamical mass sum of $3.5 M_\odot$ that appears too large, given the combined color and magnitude.

Considering the uncertainty of the orbital masses, I adopt mass estimates that are compatible with the measurements and match the expected relation between mass and absolute magnitude. Starting with the mass sum of $3.0 M_\odot$ and the well-measured mass ratio of 0.862 in the inner orbit, I fix the mass ratio in the outer orbit at $q_{AB} = 0.45$ (compatible to its measurement within the uncertainty) and obtain the component’s masses listed in Table 8. A smaller value of q_{AB} would imply that the component B is too bright for its mass.

The effective temperatures are estimated from the Dartmouth 1-Gyr isochrone using the above masses reduced by 5%. They match the combined color of the system and the “blended” $T_e = 5925 \text{ K}$ given by Casagrande et al. (2011). The modeled combined color $V - K_s = 1.48 \text{ mag}$ agrees with the measured $V - K_s = 1.49 \text{ mag}$; the model predicts $B - V = 0.63 \text{ mag}$, slightly bluer than the measured 0.69 mag . Of course, the adopted T_e remain only a plausible guess until a more detailed analysis is done to separate the individual spectra and actually measure the T_e .

The lithium line is detected in Aa and Ab, and is below the detection threshold in B. The line profiles (with the contribution of other components subtracted) are given in Figure 7 (total count 17 000 electrons, $\text{SNR}=130$). A weak FeI line at 6707.44 \AA is noticeable, as well as some asymmetry of the lithium line itself. The parameters of the Gaussian fits to the lithium line are listed in Table 8.

The inner orbit corresponds to the mass sum $M \sin^3 i = 0.91 M_\odot$. The adopted masses imply an orbital inclination of 49° , similar to the 51.5° inclination of the outer orbit. The two orbits could be nearly co-planar, although this cannot be established without resolving the inner subsystem and determining the orientation of its orbit in the sky.

The spatial velocity of HIP 13498 calculated using the γ -velocity of A,B is $(U, W, V) =$

Table 8
Components of HIP 13498

Parameter	Aa	Ab	B
Mass* (M_\odot)	1.11	0.96	0.93
M_V (mag)	4.17	5.22	5.38
T_e^* (K)	6103	5558	5443
$(B - V)^*$ (mag)	0.51	0.78	0.82
λ_{Li} (\AA)	6707.83	6707.83	...
a_{Li}	0.193	0.053	<0.01
	± 0.005	± 0.005	
σ_{Li} (km s^{-1})	6.02	6.05	...
	± 0.17	± 0.70	
EW_{Li} (m \AA)	65	18	<2
f_R^*	0.52	0.26	0.22
EW_{corr} (m \AA)	125	69	<9

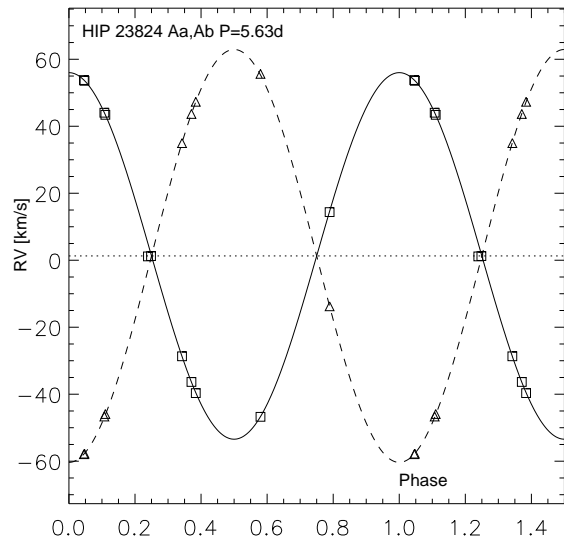


Figure 8. Spectroscopic orbit of HIP 23824 Aa,Ab, $P = 5.63 \text{ d}$. $(-37.5, -21.8, -4.3) \text{ km s}^{-1}$, placing the object in the Hyades moving group with $(U, W, V) = (-39.7, -17.7, -2.4) \text{ km s}^{-1}$, see Klutsch et al. (2014).

5. HIP 23824 (HD 35877)

The star has a spectral type F8V, $B - V = 0.57 \text{ mag}$. It is a visual binary HDS 669 with an orbital period of 26.5 yr (Tokovinin et al. 2015c). Relative photometry of the outer system A,B by speckle interferometry at SOAR gives the median magnitude differences of 2.65 and 2.20 mag at 540 and 770 nm, respectively, while $\Delta H p = 2.53 \pm 0.25 \text{ mag}$. The V -magnitudes in Table 6 correspond to $\Delta V_{AB} = 2.72 \text{ mag}$.

Double lines were noted by Nordström et al. (2004), suggesting a spectroscopic subsystem. The orbit of the subsystem Aa,Ab (Figure 8) is determined from several triple-lined CHIRON spectra. A circular orbit is forced, considering the short period; I did not subtract the outer orbit here.

The visual orbit of the outer system A,B (Figure 9) is only slightly revised by adding three recent measures to the latest published solution; all measures except the first *Hipparcos* resolution come from SOAR. The spectroscopic elements are tentative owing to the lack of the RV coverage. No additional useful RV data were found in the literature or in archives. I used the γ -velocity of

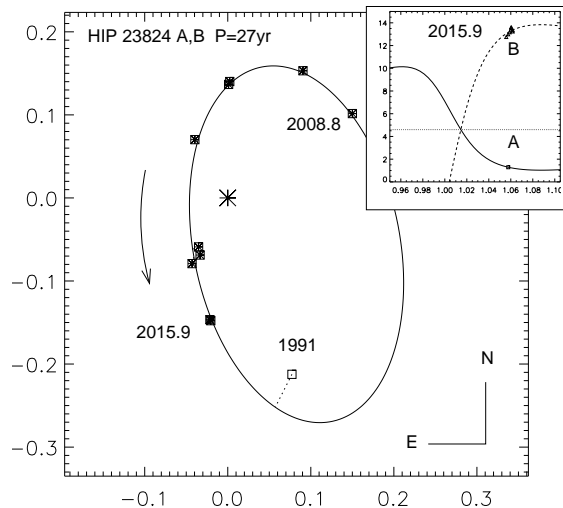


Figure 9. Orbit of HIP 23824 A,B (HDS 669), $P = 27.0$ yr, scale in arcseconds. The insert shows fragment of the RV curve.

Aa, Ab as a single measure (the CHIRON data span only 1.15 years), while the individual velocities of B show a small positive trend in agreement with the orbit. The data are not sufficient for determination of the RV amplitudes and masses. Instead, I fixed $\gamma_{AB} = 4.6$ km s $^{-1}$ to get the expected mass ratio $q_{AB} = 0.38$. Unfortunately, the periastron passage in 2014.3 has not been covered by spectroscopy, otherwise the masses could have been measured.

The HIP2 parallax of 20.8 ± 0.5 mas leads to the mass sum of $3.15 M_{\odot}$, while the RV amplitudes in the orbit of A,B correspond to the mass sum of $2.8 M_{\odot}$. In the following I adopt the mass sum of $3.0 M_{\odot}$, or a dynamical parallax of 21.2 mas. The HIP2 parallax is consistent within its error; it could be biased by the orbital motion.

The system model is adjusted to the data in the same way as for HIP 13498. Starting with the mass sum of $3.0 M_{\odot}$ and the well-measured mass ratio of 0.888 in the inner orbit, I fix the mass ratio in the outer orbit at $q_{AB} = 0.38$ and obtain the component's masses listed in Table 9. The modeled combined color $V - K_s = 1.40$ mag equals the measured one; the model predicts $B - V = 0.55$ mag, slightly bluer than measured. The adopted masses imply an inner orbital inclination of $48^{\circ}6'$, while the inclination of the outer orbit is 62° .

The lithium line is detected in Aa and Ab, while it is below the detection threshold in B, just as in HIP 13498. The parameters of the Gaussian fits to the lithium line are listed in Table 9.

The spatial velocity of HIP 23824 calculated using the γ -velocity of A,B is $(U, W, V) = (-29.4, -18.5, -4.2)$ km s $^{-1}$. A correction of $(-5.8, -4.0)$ mas yr $^{-1}$ was applied to the HIP2 proper motion to subtract the photo-center motion in the visual orbit. Eggen (1985) believes that this triple system belongs to the Hyades moving group, although the agreement of its velocity is not as good as for HIP 13498.

6. HIP 113597 (HD 217379)

This K6.5Vke star is a known $1''.9$ visual binary RST 1154 (WDS 23005–2619AB) and an X-ray source. A brighter star HIP 113579 (HD 217373) at $581''$ dis-

Table 9
Components of HIP 23824

Parameter	Aa	Ab	B
Mass* (M_{\odot})	1.15	1.02	0.83
M_V (mag)	3.89	4.72	6.20
T_e^* (K)	6227	5766	5111
$(B - V)^*$ (mag)	0.48	0.69	1.02
a_{Li}	0.119	0.044	<0.02
σ_{Li} (km s $^{-1}$)	± 0.005	± 0.005	...
EW_{Li} (mÅ)	49	20	<8
f_R^*	0.57	0.33	0.10
EW_{corr} (mÅ)	86	62	<80

tance on the sky (projected separation 18 kAU) forms with HIP 113597 a co-moving wide pair, and both objects belong to the AB Doradus group of young stars in the solar neighborhood (Zuckerman et al. 2004). The very faint companion found by Chauvin et al. (2010) at $5''.4$ from HIP 113579 remains unconfirmed, possibly not real. The WDS denotes the brighter star as C, while the visual components of RST 1154 are denoted as A and B. To avoid further confusion, I keep here the current WDS designations C, A, and B in decreasing brightness order; the unresolved photometry and spectroscopy of HIP 113597 refers to AB (C, A, B were designated hierarchically as A, Ba, and Bb in Tokovinin 2014a). Table 1 lists basic properties of this multiple system. The photometry of AB and its spectral type are from Weiss (1993). As the parallaxes of AB and C are equal within errors, in the following I adopt the average parallax of 32.6 mas.

High-resolution spectroscopy revealed HIP 113597 as a triple-lined system. This was discovered independently by Elliott et al. (2014) and Tokovinin (2015); both works are based on the echelle spectra taken in 2010 with VLT/UVES and 1.5-m/FECH, respectively. Earlier spectroscopic studies did not recognize the triple-lined nature of this object. For example, Malo et al. (2014) provide RVs of C and AB as 7.3 ± 0.3 and 6.6 ± 0.3 km s $^{-1}$, respectively, from single spectra taken with Phoenix at Gemini-South. Zuckerman et al. (2004) detected a strong lithium 6707.8Å line in the component C and noted its absence in AB (this is confirmed in the CHIRON spectra). Nordström et al. (2004) measured the constant $RV(C) = 6.10$ km s $^{-1}$ over 2135 days; they did not observe AB.

The visual binary A,B was last measured in 2015.73 with the speckle camera at SOAR, yielding the position of $239^{\circ}3', 2''30$ and the magnitude difference $\Delta I = 0.79$ mag. Its previous measurement by *Hipparcos* in 1991.25 is $235^{\circ}7', 1''839$ and $\Delta Hp = 0.79$ mag. All three components Aa, Ab, and B have comparable brightness and color, so Δm is apparently independent of the wavelength.

All three dips in the CCF are narrow (Figure 10). The central stationary component belongs to the visual secondary B, the two moving components belong to the spectroscopic subsystem Aa, Ab. The relative amplitudes of the dips are variable. This happens because the $2''.3$ separation between A and B is comparable to the $2''.7$ diameter of the CHIRON fiber projected on the sky. De-

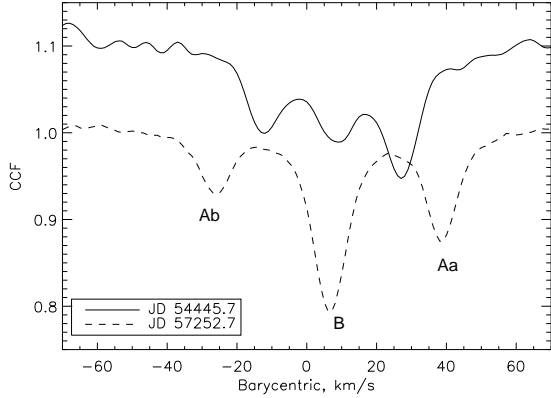


Figure 10. CCFs of HIP 113597 in two epochs. The upper curve computed from the 2010 FECH spectrum (displaced vertically by 0.1) shows that the central component belonging to B was weaker than Aa, while in most spectra taken in 2015 (lower curve) the central dip is much stronger.

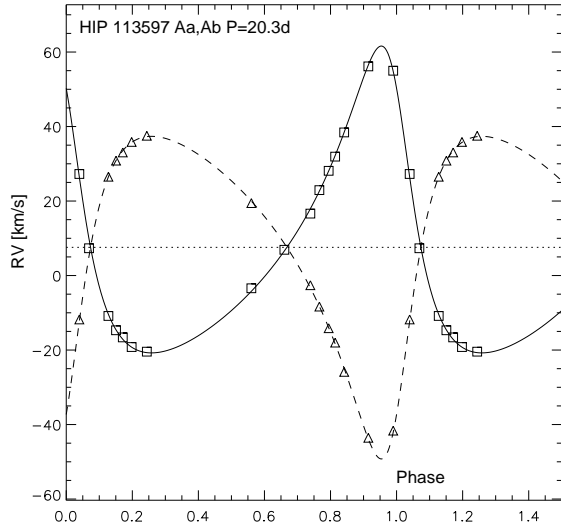


Figure 11. Spectroscopic orbit of the inner subsystem HIP 113597 Aa,Ab, $P = 20.3$ d.

pending on centering, guiding, and seeing, the fraction of the light from each component that enters the fiber is variable. In the spectra taken with FECH in 2010, the CCF area (EW) of B is half of the sum of Aa and Ab, as expected from the relative photometry of the visual binary A,B. In most spectra taken in 2015 with CHIRON, the EW(B) is comparable to the sum EW(Aa)+EW(Ab). Both instruments have the same acquisition and guiding unit; the difference in relative intensities could be caused by a different offset of the object position on the fiber.

To determine relative fluxes in the V band, I use the ratio $\text{EW}(\text{Aa})/\text{EW}(\text{Ab})=0.68\pm 0.02$, measured reliably, and assume that it reflects the light ratio (the CCF area does not depend on effective temperature at $T_e \sim 4000$ K). Assuming $\Delta V_{\text{AB}} = 0.79$ mag from *Hipparcos* photometry, I computed the apparent magnitudes of B, Aa, and Ab listed in Table 6.

Spectroscopic orbit of the inner subsystem is plotted in Figure 11. The mass ratio of the inner pair is 0.95, the spectroscopic masses $M \sin^3 i$ are 0.48 and 0.45 M_\odot . I used the RVs measured by Elliott et al. (2014) on JD

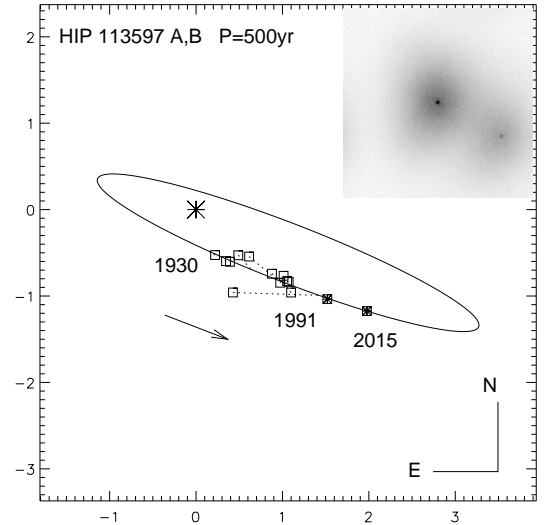


Figure 12. Tentative orbit of the pair HIP 113597 A,B (RST 1154). Visual measurements are plotted as empty squares, the *Hipparcos* and speckle data as filled squares. The insert shows the “shift-and-add” image in the I band obtained in 2015.7 at SOAR.

Table 10
Components of HIP 113597

Parameter	Aa	Ab	B
Mass* (M_\odot)	0.61	0.57	0.60
M_V (mag)	8.29	8.71	8.41
T_e^* (K)	4133	3992	4090

2455341.4055 with a correction of $+6.15$ km s^{-1} . The correction was derived by computing the center-of-mass velocity $V_A = (V_1 K_2 + V_2 K_1)/(K_1 + K_2) = 1.41$ km s^{-1} ; it must equal 7.56 km s^{-1} according to my orbit. An RV bias is expected when a semi-resolved (blended) visual binary is observed with a slit spectrograph like UVES, as guiding is made on the combined light and the individual components are no longer centered in the slit.

Knowing the absolute visual magnitudes of the components (distance modulus 2.43 mag), I estimated their masses by assuming that they are on the main sequence (the bright star C is actually on the main sequence). The result is given in Table 10. The combined magnitudes of AB in the J and K_s bands derived from this model are 7.17 and 6.33 mag, respectively. They compare well with the 2MASS magnitudes of 7.05 and 6.27. The model leads to the $B-V$ color of 1.39 mag, while the measured color is 1.34 mag (Weiss 1993). Good agreement between modeled and actual colors shows that the system indeed consists of three main-sequence stars of $\sim 0.6 M_\odot$ each. The model implies effective temperatures given in the last line of Table 10. The mass ratio in the subsystem Aa,Ab is 0.95 according to the model, matching the measured ratio. The orbital inclination of Aa,Ab is $\sim 70^\circ$.

The pair A,B has opened up from $0''.6$ to $2''.3$ since its discovery by Rossiter (1955) in 1930. We know the distance to the system and its estimated mass sum, 1.8 M_\odot . The observed motion can be represented by a visual orbit matching this mass sum (Figure 12). This orbit is *not* uniquely constrained by the data, so the errors of its

elements are undetermined. It is computed only to show that the motion is compatible with a Keplerian orbit and to get an idea of the period. Owing to the long period, no substantial improvement of this orbit is expected in the following decades.

The average $RV(B)$ is 7.05 km s^{-1} with a rms scatter of 0.54 km s^{-1} (see Table 4). The two measurements in 2010 average at 8.0 km s^{-1} , while the 13 measurements in 2015 have the average value of 6.76 km s^{-1} with a rms scatter of 0.16 km s^{-1} . It is unlikely that the difference is attributable to the different spectrographs, FECH and CHIRON, as the RVs of Aa and Ab measured from the same spectra do not show instrument-related systematics. Motion in the visual orbit is too slow to explain the RV change over five years. Elliott et al. (2014) measured $RV(B)=5.5 \text{ km s}^{-1}$ in 2010, with an uncertain bias (see above). I cannot exclude a low-mass (possibly planetary) companion to B modulating its RV. The outer orbit of A,B leaves ample room for such putative subsystem.

The positive RV difference $RV(A)-RV(B)$ in 2015 confirms the correct choice of the ascending node in this provisional orbit. I measured in 2010 $RV(C)=7.03 \text{ km s}^{-1}$ (Tokovinin 2015), in agreement with Nordström et al. (2004). Analysis of this bright component C (HIP 113579) is outside the scope of this work.

The measured RV of the component A together with the known distance and proper motion leads to the Galactic velocity of $(U, V, W) = (-3.0, -25.5, -15.1) \text{ km s}^{-1}$. A correction for the motion in the orbit A,B is not applied here; it should be small, $<1 \text{ km s}^{-1}$. According to Malo et al. (2014), the AB Doradus group has the spatial velocity $(U, V, W) = (-7.1, -27.2, -13.8) \text{ km s}^{-1}$.

The 10-yr photometric monitoring of HIP 113597 by ASAS (Pojmanski 1997)⁴ shows a constant brightness of $V = 9.58 \text{ mag}$ with an rms scatter of 0.036 mag ; it is not identified as a variable star in the ASAS database. Young $0.6 M_{\odot}$ dwarfs are expected to be active, but no flares have been detected so far. The $H\alpha$ line has a low contrast, possibly being filled by emission. The projected rotation velocity of all three components is moderate, from 7.2 to 8.8 km s^{-1} . It is faster than the estimated pseudo-synchronous rotation in the inner pair, 3.6 km s^{-1} .

7. DISCUSSION

7.1. Masses

Masses of the components of HIP 7601 are measured from the combined outer orbit with an accuracy of 2.5%. The masses of HIP 13498 are constrained by the orbit and parallax only to within $\sim 10\%$, while the masses of HIP 23824 and 113597 are not measured directly. Figure 13 plots absolute magnitude vs. mass for the first two systems. The data match empirical relations such as (Henry & McCarty 1993; Tokovinin 2014a). On the other hand, the Dartmouth 1-Gyr isochrone for solar metallicity is $\sim 0.2 \text{ mag}$ brighter; the discrepancy is even larger for $[Fe/H]=-0.15$. The agreement with the isochrone would be better for a larger-than-solar metallicity. Spectroscopic measurements of $[Fe/H]$ could have been biased by the unrecognized multiplicity.

7.2. Lithium and rotation

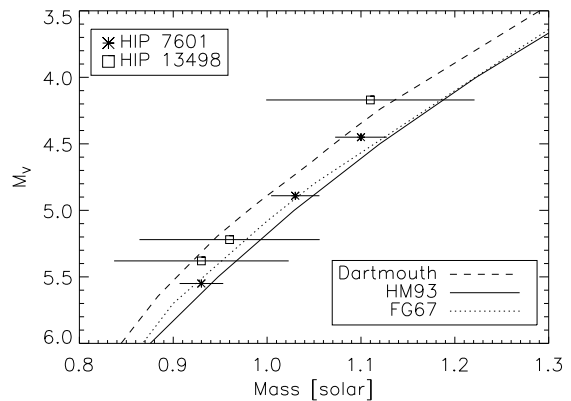


Figure 13. Relation between mass and absolute magnitude for HIP 7601 and 13498. The standard relations are traced by the dashed line (Dotter et al. 2008, solar metallicity), full line (Henry & McCarty 1993), and dotted line (Tokovinin 2014a).

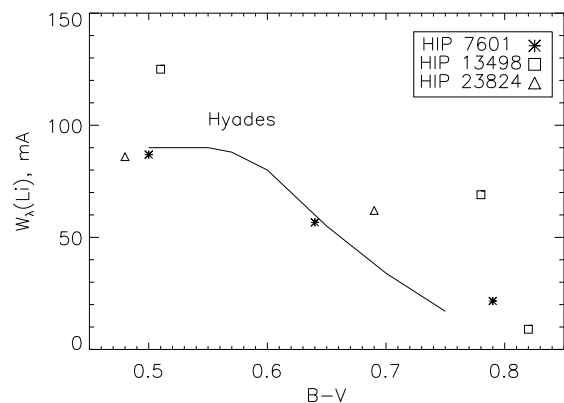


Figure 14. Equivalent width of the lithium line in the components of HIP 7601 (squares), 13498 (asterisks), and 23824 (triangles) vs. their $B-V$ color. The solid line is a schematic trend for the Hyades from Fig. 4 of Soderblom et al. (1993).

The equivalent widths of the lithium line in HIP 7601 and HIP 23824 are comparable to the stars of similar color in the Hyades (Soderblom et al. 1993), as illustrated in Figure 14, suggesting an age of $\sim 0.6 \text{ Gyr}$. However, large scatter of lithium abundance and activity indicators among stars in the Hyades makes this estimate rather uncertain. The lithium line in HIP 13498 is stronger than in the Hyades, although the system may belong to this group kinematically.

The components of both HIP 7601 and 13498 have slow axial rotation ranging from 1.8 to 4.3 km s^{-1} , as inferred from the width of their CCFs. Assuming that components of the inner subsystems are synchronized and aligned with the orbits, I estimate projected synchronous velocities of 2.0 and 2.7 km s^{-1} . They are close to the actual $V \sin i$ of the secondary components Ab, 1.8 and 2.8 km s^{-1} in HIP 7601 and 13498, respectively. The primary components Aa and the visual secondaries B rotate slightly faster. If the lines are broadened by additional factors, compared to the Sun, the above estimates are upper limits. In the closest inner binary HIP 23824 Aa,Ab, the synchronous speed of Aa, estimated at $V \sin i = 7.3 \text{ km s}^{-1}$, matches its measured rotation of 7.1 km s^{-1} , while B rotates much slower at $V \sin i = 1.6 \text{ km s}^{-1}$.

⁴ <http://www.astrouw.edu.pl/asas/>

7.3. Origin

By definition, triple-lined systems have all three components of comparable masses and luminosities. If their components were chosen randomly from the stellar mass function, SB3s would be exceptionally rare. The four nearby SB3s studied here do not appear exceptional, demonstrating that stars of similar masses are commonly assembled together in hierarchical systems. It is legitimate to ask how these objects were formed, given that the initial size of a solar-mass protostellar core, on the order of the Jeans length ($\sim 10^4$ AU), is much larger than the size of those multiples.

It is currently believed that binaries forming by fragmentation of cores or circumstellar disks have relatively large initial separations, no less than ~ 50 AU, owing to the opacity limit to fragmentation (Low & Linden-Bell 1976). Subsequent accretion shrinks the binary, while its components grow in mass. The binary separation decreases roughly as \mathcal{M}^{-2} (Bonnell & Bate 2005). The secondary grows faster than the primary, naturally leading to close pairs of comparable-mass stars. To explain the origin of a hierarchical SB3, we have to admit that the inner pair formed first and became closer, while the outer component formed later. If this triple system later gained a substantial mass and this mass was accreted preferentially by the distant companion, one expects that the former tertiary would become nearly as massive as the close pair, converting itself into a primary. Such triple systems indeed are common (e.g. κ For, Tokovinin 2013). However, in the case of SB3s the growth of the outer component had to be regulated in such a way that all three stars end up with similar masses. The challenge of explaining the formation of SB3s may lead to new insights on star formation in general.

All four systems studied here are structured in a similar way, with an inner spectroscopic pair and a tertiary companion. The orbits of those tertiaries, however, have quite different periods ranging from 1.75 yr to ~ 500 yrs. In three systems the inclinations of the inner orbits are close to the inclinations of the outer orbits, suggesting coplanarity. The inner orbit in the closest triple, HIP 7601, has a small eccentricity of $e = 0.1$. This also argues for approximate co-planarity in this system, because otherwise the Kozai-Lidov cycles (Kiseleva et al. 1998) would have increased the inner eccentricity.

On the other hand, the inner orbits in HIP 13498 and 113597 are moderately eccentric. The separations at periastron in these inner binaries correspond to equivalent circular orbits with $P_{\text{circ}} = P(1 - e)^{3/2}$ of 7.8 and 8.7 days, respectively. These periods are shorter than the 10-day circularization period of solar-type stars (Mayor et al. 2010), meaning that the components tidally interact at periastron. The Kozai-Lidov mechanism cannot be ruled out. In any case, the inner orbits will eventually become circular. These triple systems are relatively young and still evolve dynamically towards circular inner orbits. The inner binary in HIP 23824 is already circularized.

The triple system HIP 7601 holds the record of the shortest outer period (639 days) among the 4847 F- and G-type dwarfs within 67 pc of the Sun (Tokovinin 2014b). The outer periods of multiple systems in this sample are all longer than ~ 1000 days. This means that

shorter outer periods are rare. Nevertheless, such systems certainly exist. For example, VW LMi contains four solar-type stars packed in the outer orbit with a period of only 355 days (Pribulla et al. 2008). Several triple stars with short outer periods were recently found by Borkovits et al. (2016) in the *Kepler* sample of eclipsing binaries.

If the orbit of the tertiary component shrinks, at some point it starts to interact dynamically with the inner pair, even when the orbits are co-planar (no Kozai-Lidov cycles). Such interaction should start at moderate period ratios (on the order of a few tens) and may take the form of mean motion resonances (integer period ratios). The period ratio in HIP 7601 is close (although not quite equal) to an integer number. The ratio of inner periods in the hierarchical quadruple system HD 91962 is also an integer number 19.0 (Tokovinin et al. 2015b). The absence of the dust disk and outer companions to HIP 7601 imply that its outer orbit is no longer shrinking.

8. SUMMARY

Orbital elements of four hierarchical systems have been determined here, based on the original RVs and complemented by published and new resolved measurements. All objects are relatively young, as inferred from the chromospheric activity (X-ray sources), presence of lithium, and kinematics. Measurements of masses, luminosities, and rotation give an interesting material for calibrating evolution of solar-type stars and their ages.

The system HIP 7601 is most interesting, being the closest, the brightest, and with accurately determined outer orbit and masses. The accuracy of masses can be further improved by accumulating more data and/or by using better instruments. The semi-major axis of the inner 19-day subsystem is 6 mas, making it an easy target for long-baseline interferometers such as VLTI. Only a few observations are needed to establish the relative orbit orientation, confirming or refuting their suggested coplanarity. New data will also improve the accuracy of the measured masses and period ratio.

I thank the operators of the 1.5-m telescope for executing observations of this program and the SMARTS team at Yale for scheduling and pipeline processing. This work used the SIMBAD service operated by Centre des Données Stellaires (Strasbourg, France), bibliographic references from the Astrophysics Data System maintained by SAO/NASA, the Washington Double Star Catalog maintained at USNO, and products of the 2MASS survey. HIP 113597 was discussed with P. Elliott. Data from the ESO archive (program 088C.513 and its continuation) were used. Comments by anonymous Referee helped to improve the paper.

Facilities: CTIO:1.5m, SOAR

REFERENCES

- Ammler-von Eiff, M. & Reiners, A. 2012, *A&A*, 542, 116
- Bertone, E., Buzzoni, A., Chavez, M., Rodriguez-Merino, L. H., 2008, *A&A*, 485, 823
- Bonnell, I. & Bate, M. 2005, *MNRAS*, 362, 915
- Borkovits, T., Hajdu, T., Sztakovics, J. et al. 2016, *MNRAS*, 455, 4136.
- Casagrande, L., Schoenrich, R., Asplund, M. et al. 2011, *A&A*, 530, 138

- Chauvin, G., Lagrange, A.-M., Zuckerman, B. et al. 2010, *A&A*, 509, 52
- Díaz, C. G., González, J. F., Levato, H. & Grosso, M. 2011, Dotter, A., Chaboyer, B., Jevremović, D. et al. 2008, *ApJS*, 178, 89
- Eggen, O. J. 1985, *PASP*, 97, 807
- Elliott, P., Bayo, A., Melo, C. et al. 2014, *A&A*, 568, 26
- Hartkopf, W. I., Tokovinin, A., & Mason, B. D. 2012, *AJ*, 143, 42
- Henry, T. J. & McCarthy, D. W. 1993, *AJ*, 106, 773
- Henry, T., Soderblom, D., Donahue, R. A., & Baliunas, S. L. 1996, *AJ*, 111, 439
- Houk, N. 1978, Catalogue of two dimensional spectral types for the HD stars, Vol. 2. Univ. of Michigan (Ann Arbor).
- Kiseleva, L. G., Eggleton, P. P., & Mikkola, S., 1998, *MNRAS*, 300, 292
- Klutsch, A., Freire Ferrero, R., Guillout, P. et al. 2014, *A&A*, 567, 52
- Low C., Lynden-Bell D., 1976, *MNRAS*, 176, 367
- Maldonado, J., Eiroa, C., Villaver, E. et al. 2012, *A&A*, 541, 40
- Malo, L., Artigau, E., Doyon, R. et al. 2014, *ApJ*, 788, 81
- Mason, B. D., Wycoff, G. L., Hartkopf, W. I., Douglass, G. G. & Worley, C. E. 2001, *AJ*, 122, 3466 (WDS)
- Mayor, M., Udry, S., Halbwachs, J.-L., & Arenou, F. 2010, in: The formation of binary stars, Proc. IAU Symp. 200, eds. H. Zinnecker & R. Mathieu, ASP Conf. Ser., San Francisco, p. 45
- Nordström, B., Mayor, M., Andersen, J. et al. 2004, *A&A*, 418, 989 (GCS)
- Pojmanski, G., 1997, *Acta Astronomica*, 47, 467.
- Pribulla, T., Baludanský, D., Dubovský, P. et al. 2008, *MNRAS*, 390, 798
- Rossiter, R. A. 1955, *Pub. Univ. Michigan Obs.* 11, 1
- Saffe, C., Gomez, M., Pintado, O., & Gonzalez, E. 2008, *A&A*, 490, 297
- Smith, R., Wyatt, M. C., & Dent, W. R. F. 2008, *A&A*, 485, 897
- Soderblom, D., Pilachowski, C. A., Fedele, S. B. et al. 1993, *AJ*, 105, 2299
- Tokovinin, A. 2013, *AJ*, 145, 76
- Tokovinin, A., Fischer, D. A., Bonati, M. et al. 2013, *PASP*, 125, 1336
- Tokovinin, A. *AJ*, 2014a, 147, 86
- Tokovinin, A. *AJ*, 2014b, 147, 87
- Tokovinin, A., Pribulla, T., & Fischer, D. 2015a, *AJ*, 149, 8
- Tokovinin, A., Latham, D. W., & Mason, B. D. 2015b, *AJ*, 149, 195
- Tokovinin, A., Mason, B. D., Hartkopf, W. I. et al. 2015c, *AJ*, 150, 50
- Tokovinin, A. 2015, *AJ*, 150, 177
- Torres, C. A. O., Quast, G. R., Da Silva, L. et al. 2006, *A&A*, 460, 695
- Trilling, D. E., Bryden, G., Beichman, C. A. et al. 2008, *ApJ*, 674, 1086
- van Leeuwen, F. 2007, *A&A*, 474, 653 (HIP2)
- Weis, E. W. 1993, *AJ*, 105, 1962
- Wichman, R., Schmitt, J. H. M. M., & Hubrig, S. 2003, *A&A*, 400, 293
- Zuckerman, B., Song, I., & Bessell, M. S. 2004, *ApJ*, 613, L65

Table 4
Radial velocities and residuals

HIP	System	Date (JD -2400000)	V_1	σ_1 (km s ⁻¹)	(O-C) ₁	V_2	σ_2 (km s ⁻¹)	(O-C) ₂	Ref. ^a
7601	Aa,Ab	54855.5390	20.426	0.100	0.147	-24.180	0.200	-0.080	H
7601	Aa,Ab	54856.5450	12.032	0.100	0.206	H
7601	Aa,Ab	54859.5670	-17.230	9.900	0.305	20.933	0.200	0.094	H
7601	Aa,Ab	55563.5520	-14.128	0.100	0.090	16.785	0.200	-0.112	H
7601	Aa,Ab	55563.6090	-13.323	0.100	0.111	H
7601	Aa,Ab	55978.4900	24.451	0.100	-0.074	-29.116	0.200	0.031	H
7601	Aa,Ab	55978.4950	24.405	0.100	-0.086	-29.264	0.200	-0.158	H
7601	Aa,Ab	56269.7090	19.545	0.100	-0.215	-23.685	0.200	-0.201	C
7601	Aa,Ab	56896.8140	-38.118	0.100	-0.052	45.101	0.150	-0.138	C
7601	Aa,Ab	56987.5270	10.661	0.100	0.115	-12.509	0.150	0.024	C
7601	Aa,Ab	56987.5280	10.621	0.100	0.084	-12.517	0.150	0.005	C
7601	Aa,Ab	56991.5900	-27.930	0.100	0.017	33.067	2.000	-0.147	C
7601	Aa,Ab	56994.5770	-37.149	0.100	-0.179	44.112	0.150	0.175	C
7601	Aa,Ab	57175.9430	33.623	0.100	0.084	-40.053	0.100	-0.193	C
7601	Aa,Ab	57226.7530	-37.633	0.100	0.111	44.691	0.150	-0.166	C
7601	Aa,Ab	57284.8840	-37.582	0.100	0.126	44.774	0.150	-0.040	C
7601	Aa,Ab	57352.5730	31.592	0.100	-0.004	-37.246	0.150	0.304	C
7601	Aa,Ab	57365.5720	-7.403	0.100	-0.087	8.838	0.150	0.144	C
7601	Aa,Ab	57402.5990	-28.871	0.100	-0.028	34.134	0.150	-0.145	C
7601	A,B	51845.2470	-12.060	2.000	-0.009	18.700	1.000	-0.110	W
7601	A,B	54782.5586	6.040	1.000	0.580	-15.950	1.000	-0.308	L
7601	A,B	54855.5386	2.225	0.080	0.171	-9.147	0.200	-0.207	H
7601	A,B	54859.5670	1.715	0.080	-0.034	-7.980	0.200	0.362	H
7601	A,B	55563.5516	-4.915	0.080	-0.107	4.904	9.900	0.345	H
7601	A,B	55978.4901	5.445	0.080	-0.130	-15.558	0.200	0.310	H
7601	A,B	55978.4951	5.478	0.080	-0.097	-15.797	0.200	0.071	H
7601	A,B	56269.7094	-11.455	0.080	-0.009	17.635	0.200	0.018	H
7601	A,B	56896.8139	-10.712	0.080	-0.041	16.253	0.150	0.159	C
7601	A,B	56987.5272	-10.391	0.080	0.034	15.600	0.150	-0.010	C
7601	A,B	56987.5280	-10.365	0.080	0.060	15.579	0.150	-0.031	C
7601	A,B	56991.5905	-10.168	0.080	-0.021	15.056	0.150	-0.006	C
7601	A,B	56994.5775	-9.903	0.080	0.032	14.519	0.150	-0.126	C
7601	A,B	57175.9426	2.928	0.080	-0.087	-10.800	0.150	0.033	C
7601	A,B	57226.7528	4.950	0.080	0.034	-14.626	0.150	-0.054	C
7601	A,B	57284.8841	5.990	0.080	0.100	-16.544	0.150	-0.055	C
7601	A,B	57352.5726	5.147	0.080	0.096	-14.870	0.150	-0.032	C
7601	A,B	57365.5723	4.613	0.080	0.028	-14.057	0.150	-0.136	C
7601	A,B	57402.5989	2.558	0.080	-0.043	-10.026	0.150	-0.009	C
13498	Aa,Ab	54781.7194	-28.948	0.500	-0.009	33.452	0.500	-0.119	C
13498	Aa,Ab	56910.8509	-26.499	0.050	0.012	30.725	0.050	-0.030	C
13498	Aa,Ab	56938.8271	-27.214	0.050	-0.060	31.456	0.050	-0.044	C
13498	Aa,Ab	57003.7262	17.868	0.050	0.044	-20.594	0.050	0.083	C
13498	Aa,Ab	57008.7007	-28.481	0.050	-0.031	32.983	0.050	-0.021	C
13498	Aa,Ab	57010.7707	-20.229	0.050	0.007	23.464	0.050	-0.010	C
13498	Aa,Ab	57015.6590	51.560	0.050	-0.051	-59.917	0.050	-0.045	C
13498	Aa,Ab	57319.6708	-25.755	0.050	0.047	29.915	0.050	-0.017	C
13498	Aa,Ab	57333.6875	-26.047	0.050	0.031	30.299	0.050	0.048	C
13498	A,B	51847.307	19.650	5.000	0.306	16.700	5.000	-0.079	W
13498	A,B	54781.7194	20.430	0.500	0.006	14.340	0.500	0.257	L
13498	A,B	56910.8510	17.816	0.040	0.004	20.613	0.040	0.010	C
13498	A,B	56938.8270	17.762	0.040	-0.043	20.581	0.040	-0.038	C
13498	A,B	57003.7260	17.853	0.040	0.063	20.822	0.150	0.167	C
13498	A,B	57008.7010	17.769	0.040	-0.020	20.650	0.040	-0.008	C
13498	A,B	57010.7710	17.792	0.040	0.003	20.646	0.040	-0.013	C
13498	A,B	57015.6590	17.736	0.040	-0.051	20.712	0.040	0.050	C
13498	A,B	57319.6710	17.737	0.040	0.007	20.852	0.040	0.048	C
13498	A,B	57333.6880	17.755	0.040	0.027	20.793	0.040	-0.017	C
23824	Aa,Ab	57258.8734	14.375	0.500	-0.186	-13.756	0.500	-0.100	C
23824	Aa,Ab	57333.8850	43.417	0.500	0.013	-45.911	0.500	0.237	C
23824	Aa,Ab	57350.7610	44.042	0.500	-0.015	-46.657	0.500	0.227	C
23824	Aa,Ab	57364.6842	-46.749	0.500	-0.062	55.650	0.500	0.308	C
23824	Aa,Ab	57374.6089	-28.670	0.500	0.029	34.973	0.500	-0.105	C
23824	Aa,Ab	57378.5676	53.788	0.500	-0.014	-57.912	0.500	-0.051	C
23824	Aa,Ab	57378.5777	53.567	0.500	-0.058	-57.742	0.500	-0.080	C
23824	Aa,Ab	57379.6591	1.240	2.500	-0.564	1.150	9.500	-3.856	C
23824	Aa,Ab	57391.6627	-36.338	0.500	0.049	43.675	0.500	-0.064	C
23824	Aa,Ab	57391.7363	-39.662	0.500	-0.147	47.314	0.500	0.052	C
23824	A,B	57333.8850	12.751	0.200	-0.301	C
23824	A,B	57350.7610	12.989	0.200	-0.167	C
23824	A,B	57364.6842	1.290	0.200	-0.003	13.166	0.200	-0.068	C
23824	A,B	57374.6089	13.406	0.200	0.121	C
23824	A,B	57378.5676	13.622	0.200	0.317	C
23824	A,B	57378.5777	13.558	0.200	0.253	C
23824	A,B	57391.6627	13.238	0.200	-0.128	C

Table 4 — *Continued*

HIP	System	Date (JD - 2400000)	V_1	σ_1 (km s ⁻¹)	(O-C) ₁	V_2	σ_2 (km s ⁻¹)	(O-C) ₂	Ref. ^a
23824	A,B	57391.7363	13.350	0.200	-0.017	C
113597	Aa,Ab	55341.4035	56.140	1.000	-0.228	-43.560	1.000	0.730	E
113597	Aa,Ab	55444.6827	54.973	0.500	0.312	-41.635	0.500	0.841	F
113597	Aa,Ab	55445.6957	27.253	0.500	1.041	-11.788	0.500	0.467	F
113597	Aa,Ab	57218.7357	-16.610	1.500	0.368	33.040	1.500	-0.586	C
113597	Aa,Ab	57226.6538	-3.420	1.500	0.796	19.440	1.500	-0.629	C
113597	Aa,Ab	57228.6877	6.910	5.000	0.387	C
113597	Aa,Ab	57250.6373	16.618	0.500	-1.144	-2.600	1.500	0.679	C
113597	Aa,Ab	57251.7665	28.105	0.500	0.228	-14.146	0.500	-0.122	C
113597	Aa,Ab	57252.7201	38.411	0.500	0.177	-25.867	0.500	-0.841	C
113597	Aa,Ab	57277.7028	7.325	5.200	-2.327	C
113597	Aa,Ab	57299.7150	-14.700	1.000	-0.219	30.850	0.500	-0.123	C
113597	Aa,Ab	57300.6760	-19.200	0.500	-0.144	35.870	0.500	0.037	C
113597	Aa,Ab	57301.6130	-20.440	0.500	0.071	37.520	0.500	0.142	C
113597	Aa,Ab	57319.5924	-10.857	0.500	-0.504	26.531	0.500	-0.056	C
113597	Aa,Ab	57332.5887	22.925	0.500	0.456	-8.337	0.500	-0.058	C
113597	Aa,Ab	57333.5621	31.921	0.500	-0.083	-18.005	0.500	0.403	C
113597	Aa,Ab	57364.5277	-18.394	0.500	0.596	35.434	0.500	-0.329	C
113597	Aa,Ab	57377.5298	58.780	0.500	-0.573	-48.380	0.500	-0.919	C
113597	B	55444.6827	7.719	F
113597	B	55445.6957	8.290	F
113597	B	57218.7357	6.517	C
113597	B	57226.6538	7.070	C
113597	B	57228.6877	6.912	C
113597	B	57251.7665	6.857	C
113597	B	57252.7201	6.752	C
113597	B	57299.7157	6.542	C
113597	B	57300.6762	6.803	C
113597	B	57301.6131	6.722	C
113597	B	57319.5924	6.661	C
113597	B	57332.5887	6.979	C
113597	B	57333.5621	6.746	C
113597	B	57364.5277	6.608	C
113597	B	57377.5298	6.722	C

^a C: CHIRON; E: Elliott et al. (2014); F: FECH; H: HARPS; L: Tokovinin (2015); W: Wichman et al. (2003).Table 5
Position measurements and residuals

HIP	System	Date (yr)	θ ($^\circ$)	ρ ($''$)	σ ($''$)	(O-C) _{θ} ($^\circ$)	(O-C) _{ρ} ($''$)	Ref. ^a
7601	A,B	2011.0366	50.2	0.0378	0.020	-3.7	-0.0096	SOAR
7601	A,B	2011.0366	53.4	0.0488	0.010	-0.5	0.0014	SOAR
7601	A,B	2014.7661	113.0	0.0640	0.001	-3.0	-0.0004	SOAR
7601	A,B	2014.8535	132.4	0.0630	0.001	-1.0	-0.0013	SOAR
7601	A,B	2015.0286	173.3	0.0586	0.001	-0.3	0.0022	SOAR
7601	A,B	2015.0286	173.3	0.0574	0.001	-0.3	0.0010	SOAR
7601	A,B	2015.1051	194.8	0.0564	0.001	0.4	0.0013	SOAR
7601	A,B	2015.1713	212.0	0.0548	0.001	-0.2	-0.0020	SOAR
7601	A,B	2015.2504	231.4	0.0620	0.001	0.3	0.0000	SOAR
7601	A,B	2015.4976	270.9	0.0826	0.001	0.4	-0.0014	SOAR
7601	A,B	2015.7377	296.1	0.0917	0.001	0.4	0.0009	SOAR
7601	A,B	2015.9102	315.7	0.0806	0.001	0.7	0.0006	SOAR
7601	A,B	2016.0475	337.0	0.0624	0.001	-0.4	-0.0008	SOAR
7601	A,B	2016.1344	360.1	0.0524	0.001	0.6	0.0001	SOAR
13498	A,B	1927.0200	126.4	0.390	1.050	0.3	-0.125	Vis
13498	A,B	1933.0000	134.2	0.460	0.050	2.3	-0.043	Vis
13498	A,B	1936.7000	134.5	0.410	0.050	-1.3	-0.063	Vis
13498	A,B	1938.8400	138.1	0.420	0.050	-0.2	-0.028	Vis
13498	A,B	1946.7300	145.4	0.300	0.050	-7.2	0.000	Vis
13498	A,B	1960.8800	95.5	0.250	0.050	-2.0	0.015	Vis
13498	A,B	1975.7230	123.9	0.460	0.050	0.5	-0.045	Vis
13498	A,B	1978.7960	128.2	0.530	0.050	1.8	0.015	Vis
13498	A,B	1989.9330	137.7	0.452	0.005	-0.2	-0.001	Vis
13498	A,B	1990.0500	137.3	0.310	1.050	-0.7	-0.142	Vis
13498	A,B	1990.9160	139.2	0.444	0.005	0.1	0.004	Spe
13498	A,B	1991.2500	140.0	0.437	0.010	0.5	0.002	Hip
13498	A,B	1991.6000	133.4	0.450	0.050	-6.6	0.020	Vis
13498	A,B	1991.7130	140.0	0.427	0.005	-0.2	-0.002	Spe
13498	A,B	2010.9660	88.7	0.179	0.002	-0.4	0.000	SOAR
13498	A,B	2014.7690	107.6	0.316	0.005	1.9	0.003	SOAR
13498	A,B	2015.0290	106.2	0.320	0.002	-0.1	-0.001	SOAR

Table 5 — *Continued*

HIP	System	Date (yr)	θ ($^{\circ}$)	ρ ($''$)	σ ($''$)	$(O-C)_{\theta}$ ($^{\circ}$)	$(O-C)_{\rho}$ ($''$)	Ref. ^a
23824	A,B	1991.2500	200.0	0.226	0.020	7.2	-0.032	SOAR
23824	A,B	2008.7729	304.1	0.181	0.002	-0.2	0.002	SOAR
23824	A,B	2010.9684	329.4	0.178	0.005	0.1	0.002	SOAR
23824	A,B	2013.1283	359.6	0.137	0.003	0.6	-0.000	SOAR
23824	A,B	2013.1283	359.0	0.140	0.002	0.0	0.003	SOAR
23824	A,B	2014.0430	29.4	0.081	0.003	0.7	0.004	SOAR
23824	A,B	2015.0286	149.2	0.069	0.002	3.8	-0.006	SOAR
23824	A,B	2015.0286	154.1	0.076	0.003	8.7	0.002	SOAR
23824	A,B	2015.1051	151.5	0.090	0.007	1.5	0.008	SOAR
23824	A,B	2015.9102	172.1	0.149	0.003	-0.9	-0.001	SOAR
23824	A,B	2015.9102	171.7	0.148	0.002	-1.4	-0.003	SOAR
113597	A,B	1930.2000	202.7	0.570	0.050	6.0	0.070	Vis
113597	A,B	1935.8500	210.2	0.690	0.050	2.7	0.081	Vis
113597	A,B	1941.3300	213.0	0.720	0.050	-1.6	-0.006	Vis
113597	A,B	1950.8600	222.8	0.720	0.050	0.2	-0.221	Vis
113597	A,B	1963.8000	228.5	0.820	0.100	-0.5	-0.417	Vis
113597	A,B	1965.8400	229.0	1.290	0.100	-0.8	0.007	Vis
113597	A,B	1966.6200	229.8	1.150	0.100	-0.2	-0.151	Vis
113597	A,B	1966.8200	228.9	1.460	0.100	-1.2	0.155	Vis
113597	A,B	1966.8500	232.9	1.270	0.100	2.8	-0.036	Vis
113597	A,B	1967.4900	232.0	1.360	0.100	1.7	0.040	Vis
113597	A,B	1970.5500	231.9	1.340	0.100	0.6	-0.048	Vis
113597	A,B	1986.5700	204.0	1.050	9.500	-31.1	-0.685	Vis
113597	A,B	1991.2500	235.7	1.839	0.010	-0.3	0.008	Hip
113597	A,B	2015.7380	239.3	2.300	0.005	0.0	-0.001	SOAR

^a HIP: Hipparcos; SOAR: speckle interferometry at SOAR; Spe: speckle interferometry at other telescopes ; Vis: visual micrometer measures.